energies

MDPI

Article

New Insights into Flow for a Low-Bypass-Ratio Transonic Fan with Optimized Rotor

Mingjun Liu [1], Zhenjiu Zhang [1], Zhuoming Liang [2], Haibing Xiao [1], Huanlong Chen [2,*], Xianqing Yang [3] and Changxiao Shao [4]

[1] Shenzhen Institute of Information Technology, Shenzhen 518172, China; liumj@sziit.edu.cn (M.L.); zhangzhenjiu@sziit.edu.cn (Z.Z.); xiaohb@sziit.edu.cn (H.X.)
[2] Harbin Institute of Technology, Harbin 150001, China; hgdlzm@126.com
[3] Yobow Turbofan (Shenzhen) Co., Ltd., Shenzhen 518055, China; yang.xianqing@yobow.cn
[4] Harbin Institute of Technology (Shenzhen), Shenzhen 518055, China; shaochangxiao@hit.edu.cn
* Correspondence: chenhuanlong@126.com

Abstract: In this paper, a three-dimensional aerodynamics optimization system is built and applied to optimize a rotor blade to balance the conflicts between stall margin, total pressure ratio, adiabatic efficiency, and mass flow rate for the high-loading and transonic-flow fan. A novel flow diagnostic method based on vorticity dynamics theory is utilized to analyze the reasons for the improvement in aerodynamic performance in the optimized transonic fan. In the established aerodynamic optimization method, use the blade profile camber line curvature and its leading edge metal angle as the optimization variables, which are optimized by modifying the coordinates of their control points and introducing a genetic algorithm. Finally, the vorticity dynamics parameters, such as the boundary vorticity flux (BVF), azimuthal vorticity and skin-friction lines are used to diagnose the key flow features in the optimized and baseline fan passage. The results indicate that, by controlling skillfully the blade camber line curvature in the optimization improves the aerodynamic performance of the fan stage, increasing the total pressure ratio by 1.90% while increasing the mass flow rate and adiabatic efficiency by 5.82% and 4.45%, respectively. The formulas from the vorticity dynamics diagnosis method indicate a close link between the aerodynamic performance and vorticity dynamic parameters for the axial fan/compressor passage flow, and that both azimuthal vorticity and boundary vorticity flux have significant influence on fan stage performance. Moreover, the boundary layer separation flow on the rotor blade surface is accompanied by a spike of entropy and static pressure, and their derivative/gradient also suffer drastic changes under the effect of shock waves. Detailed flow information can be obtained about the on-wall with high accuracy based on the vorticity dynamics diagnosis method, which provides researchers with a novel method for the turbomachinery aerodynamic design and analysis in the aero-engine engineering development field.

Keywords: low-bypass-ratio transonic fan; aerodynamic optimization; vortex dynamics; secondary flow; shock wave

check for updates

Citation: Liu, M.; Zhang, Z.; Liang, Z.; Xiao, H.; Chen, H.; Yang, X.; Shao, C. New Insights into Flow for a Low-Bypass-Ratio Transonic Fan with Optimized Rotor. *Energies* **2023**, *16*, 7230. https://doi.org/10.3390/en16217230

Academic Editors: Davide Di Battista, Fabio Fatigati and Marco Di Bartolomeo

Received: 2 October 2023
Revised: 20 October 2023
Accepted: 22 October 2023
Published: 24 October 2023

Copyright: © 2023 by the authors. Licensee MDPI, Basel, Switzerland. This article is an open access article distributed under the terms and conditions of the Creative Commons Attribution (CC BY) license (https://creativecommons.org/licenses/by/4.0/).

1. Introduction

As a highly integrated flow system, the overall performance of modern aircraft engines depends on the excellent matching of various functional parts, and every working unit is required to serve the whole system. Therefore, being the first part of a turbofan engine, the fan stage needs to be designed with advanced technologies to enhance its loading and efficiency while extending its stall margin. Under this background, design theories and techniques are being proposed all of the way along the development line of turbomachinery while numerous design platforms have been built over the last few decades. Quasi-3D blade design and flow analysis technique is the foundation of modern 3D design techniques, and its origin could be traced back to the 1950s when Wu [1] proposed the concept of

S1/S2 stream surfaces. On the basis of this theory, a lot of solution methods are put forward with the streamline curvature method and the throughflow matrix method as representatives [2,3]. These quasi-3D blade design techniques could provide favorable initial schemes for further design, but the inevitable dependency on experimental data has restricted their further development. On the other hand, with the development of computer science and computational fluid dynamics, modern 3D design and analysis techniques based on RANS methods have been developed, with which the disadvantages of quasi-3D design techniques have been settled successfully. Furthermore, the application of 3D design techniques in turbomachinery has prompted the emergence of a number of advanced theories including swept and leaned blade configurations. One of the typical designs is the low-noise transonic fan QF-12 which adopted the concept of swept blade [4,5]. Similarly, Wennerstorm [6,7] introduced swept blade into the design of a high through-flow transonic fan stage and received favorable effects, while a series of experiments were done by the Wright-Patterson Air Force Base in order to investigate the influence of blade sweep on the performance of the compressor [8,9]. Denton et al. [10] studied the effects of leaned and swept blade on a transonic fan, researchers in China have also conducted relevant studies [11,12]. Ceyrosky et al. [13] studied the influence of the volute in the triggering of instability phenomena through a CFD investigation. Cravero et al. [14] identifies the flow phenomena that trigger instability of a two stage back-to-back radial compressor through unsteady simulation.

It is obvious that the geometrical feature of blade passage has a significant influence on the aerodynamic performance of fan/compressor. However, restricted by the deficiency of design techniques, early investigations in blade optimization could only concentrate on one or few geometry features, which are not enough to satisfy the demands of practical engineering problems. Consequently, the design systems that have high efficiency and strong fault-tolerant ability are currently in great need. Many investigators have been devoted to this problem and lots of contributions have been made. Optimizations for the famous NASA Rotor 37 blade passage was done by Benini [15] and Jang et al. [16] respectively, while the NASA Rotor 67 blade passage was optimized by Lian et al. [17] using a multi-objective optimization method, the stage weight was decreased and the total pressure ratio was increased through their study. One of the other challenges that highly-load compression systems are faced with is the maintenance of the stall margin (SM > 10~15%). In the optimization work by Ellbrant et al. [18,19], a trade-off between efficiency and stall margin was made in a transonic compressor stage. Besides, the adiabatic efficiency for the NASA Rotor 67 blade was increased by 2% over the entire operating range by the redesign work conducted by Oyama et al. [20]. Recently, Mark et al. [21–27] has established a novel turbomachinery aerodynamic optimization design system. Based on the control of curvature for the blade geometry, the optimization system could couple the optimization and the CFD solver successfully, which was able to prove its outstanding engineering practicability in engineering application. Moreover, the optimization design is also important on the uncertainty quantification [28,29].

At present, scholars in the field of aerodynamic design of compressor/fan generally consider that the effect of air humidity on the performance of compressor/fan is weak within a small range of humidity and temperature changes. However, under the conditions of high humidity and flow rate, the water vapor in the wet air condense on the surfaces of the blade, and even enhance condensation excitation, which interferes with the original wave system structure of the compressor flow passage [30–33]. Bertoneri et al. [34] studied the performance of a two-stage centrifugal compressor under wet air conditions, and the results showed that when the fluid changes from dry air to wet air, the pressure ratio was increased, and the temperature ratio and the polytropic efficiency were dropped. In this paper, the effect of humidity on the aerodynamic performance of the compressor/fan is ignored in the aerodynamic design process in order to facilitate the application of existing compressor design theories and reduce the difficulty of data analysis. The utilization of the

real gas model may make difficulties in the calculation of CFD numerical simulation, such as the calculation of stability, convergence and computational efficiency.

The formation and development of vortex structures is inevitable during the evolution of viscous flows in the fan/compressor passage, and these flow configurations are closely linked with the aerodynamic performance of the fan/compressor. The vortex structures could give important clues about the flow features in aircraft engines and work as a guidance for aerodynamic optimizations. Vorticity dynamics diagnostic methods are developed to investigate the flow according to the derivative/gradient of flow parameters [35,36]. The vorticity dynamics diagnostic method, which focuses on crucial physical principles and distinctive parameters like the boundary vorticity flux (BVF), vorticity/skin-friction vectors, and azimuthal vorticity, is an insightful aerodynamic analysis/design technique and could offer the designer completely original concepts outside of conventional design principles [37–39]. Investigations in this technique have obtained valuable results and further studies are expected.

There are lots of factors that could affect the performance of the fan/compressor, and the conflict between these factors would become particularly pronounced when it comes to a low bypass-ratio transonic fan stage whose hub-to-tip ratio is relatively low. Hence, a proper balance of the performance index is of great significance to maximize the overall performance of the fan stage. With the challenges above, this study implements the optimization of the rotor blade for a low bypass-ratio transonic fan under stage flow conditions. The aim of the design is to raise the fan's mass flow rate and total pressure ratio when its efficiency and stall margin remain unchanged. To acquire a comprehensive of the process for transonic flow control, vorticity diagnostic methods are applied to discuss the flow. In this paper, the optimization process will be described in detail and the origin of various flow structures and their influence will be interpreted in depth using vorticity diagnostic methods.

2. Optimization System

The turbomachinery aerodynamic optimization design system employed in this paper is developed by Mark et al. [21–27] under the Linux framework. It is made up of Shell scripts, Python scripts and Fortran executable files. The schematic diagram of the optimization system is shown in Figure 1. There are three main parts in the design system: the user-defined module, the optimization script module and the Dakota optimization module. The user-defined module is executed only once in each optimization. Its main goal is to parameterize the geometry and to define the boundary conditions as well as the optimization variables using the journal files it contains. Once the optimization target is defined, the optimization script would execute the three-dimensional blade geometry builder (3DBGB) code automatically to produce the blade. The generated 3D blade geometry is in the form of the geometry input file *.geomTurbo and would get meshed by the grid generator called Autogrid5. Then, the mesh is transmitted to the CFD solver Fine/Turbo and the calculation results are collected and sent to Dakota. After each optimization step, Dakota would analyze the results automatically and extract the value of the objective function. Furthermore, based on the results from the last optimization step, Dakota would decide on the parameters in the next scheme using genetic algorithm so as to keep the optimization system running continuously.

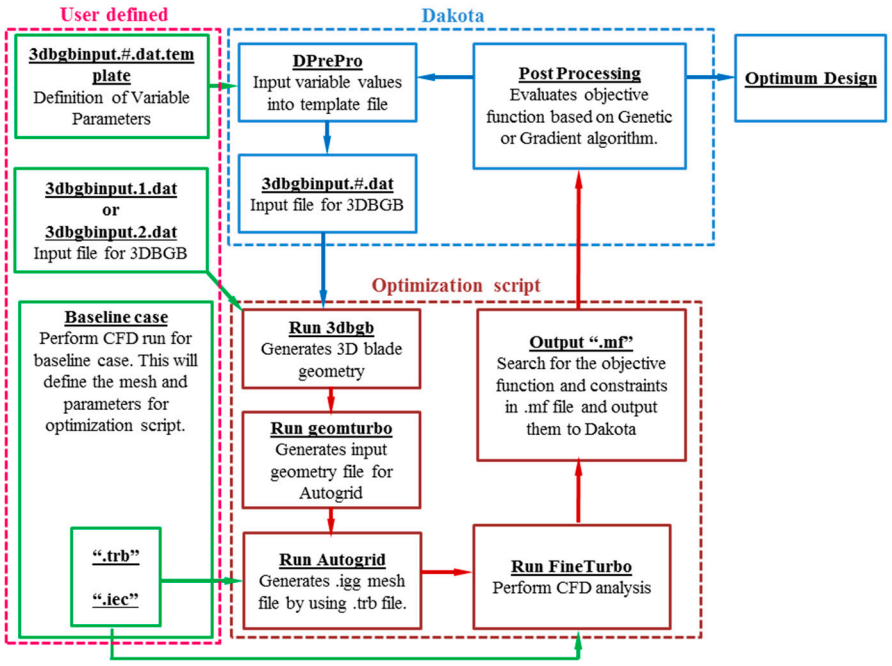


Figure 1. Optimization schematic.

In order to ensure the smoothness of the blade, cubic B-spline is employed when building the 3D geometry. Meanwhile, the geometrical parameters of the blade such as the curvature of the camber line and the inlet/outlet angles are modified so that diversified blade configurations could be produced. Additionally, the matching of the flow characteristics between different blade rows is also taken into consideration in the optimization system. Specific explanations about the geometric modeling process could be found in Refs. [21,22,26], the optimization process is also expounded in Ref. [21], open executables codes of the optimization modules are available online (http://gtsl.ase.uc.edu/3DBGB/ (accessed on 10 February 2023)).

Considering the features in both prediction precision and numerical stability, the Spalart-Allmaras turbulence model is chosen for the numerical simulations in the present study. The blade geometry in the baseline case (denoted as Baseline) is designed by a Turbomachinery Axisymmetric design code (known as T-AXI) [27] and the geometry generator 3DBGB [23], while the flow path is inherited from a transonic fan which has been tested by experiments [40]. Geometry and meshes for the baseline stage are displayed in Figure 2. Although the optimization is merely limited to the rotor blade, the flow in the whole stage is calculated and the total grid number is approximately 1.25 million. As shown in Table 1, the relative variation of mass flow rate is not larger than 0.08% when the total grid number exceeds 1.25 million, further increase in total grid number would only increase the relative change. Furthermore, the y+ of the first grid cell is guaranteed to be less than 5 in order that the boundary layer's flow details could be depicted accurately A total temperature of 288.15 K, total pressure of 101,325 Pa, and flow direction are imposed to the inlet plane of the computational domain, and the static pressure is imposed to the outlet by simple radial equilibrium relation as the boundary condition. In addition, the solid boundaries are subject to the adiabatic non-slipping condition. The mixing-plane method is employed to transmit flow parameters between blade rows. Main design parameters for the fan stage are presented in Table 2. These data indicate that this is a high-load (stage load factor greater than 0.34) and high-throughflow (flow coefficient greater than 0.44) type of low-bypass-ratio transonic fan, in which the design of the total pressure ratio and adiabatic efficiency in the same type of fan belong to the higher level of technology. It is necessary to carry out the relevant flow matching study using the aerodynamic optimization design technique coupled with the CFD method so as to obtain the transonic fan throughflow

structure that satisfies the expected design requirements. The related throughflow structure of the fan is shown in Figure 2. The research object of this paper is to meet the technical requirements of a new aero-engine, which needs to improve the flow rate and total pressure ratio at the design point while ensuring that the geometric dimension of the fan meridian passage unchanged.

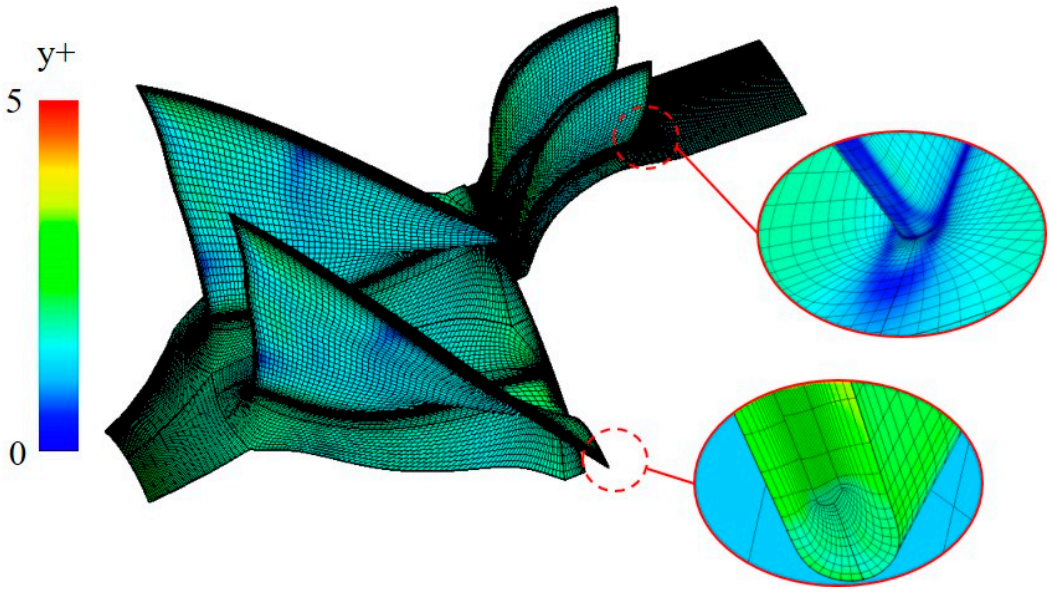


Figure 2. Geometry and meshes for the baseline fan stage.

Table 1. Information of grid independence.

Case	Grid Distribution (Streamwise × Pitchwise × Radial)		Total Grid Cell Number	Performance Parameters		
	Rotor	Stator		Efficiency	Pressure Ratio	Mass Flow Rate
1	39 × 11 × 75	43 × 11 × 75	768,754	0.88596	1.9735	8.8543
2	59 × 19 × 75	63 × 19 × 75	1,250,734	0.88879	1.9743	8.8586
3	71 × 23 × 75	75 × 23 × 75	1,512,658	0.88913	1.9739	8.8611
4	111 × 37 × 75	119 × 37 × 75	2,595,228	0.88905	1.9740	8.8607

Table 2. Parameters of the redesigned fan stage.

Parameter	Value
Number of rotor and stator blade	13, 36
Mach number in relative coordinates for rotor blade tip	1.3848
Loading coefficient for rotor blade tip	0.463
Flow coefficient for rotor blade tip	0.500
Hub-to-tip ratio of the rotor passage	0.460
Corrected design angular velocity (rpm)	28,000.0
Corrected rotor tip tangent velocity (m/s)	410.0
Clearance for rotor blade tip (mm)	0.50
Mass flow rate at design angular velocity for fan (kg/s)	≥9.34
Adiabatic efficiency at design-point	≥0.87
Total pressure ratio at design-point	≥2.05

3. Rotor Blade Optimization

There exist two steps in the process of rotor blade optimization. The first is to optimize the camber line of the rotor blade (denoted as Camber_Opt) and the next is to match the

leading edge blade angles (denoted as Angle_Opt). The curvature of the camber line is established by the cubic B-spline formula according to numerous control points in the current optimization system, and the camber line is adjusted by modifying the variations of these control points. Since the curvature of a curve is numerically approximate to its second derivative, the curvature obtained here could be considered equivalent to the second derivative of the camber line. In other words, the camber line could be acquired through the double integration of the defined curvature (which is just the way we do it in this study). In consideration of computational time and efficiency, five spanwise positions are chosen as the optimization plane. In addition, four variables are defined in each optimization plane. They represent the chordwise location of the control point and the curvature values for the camber line at the specified location. The constraint conditions are as follows:

Maximize: adiabatic efficiency η^* on the highest efficiency point for fan-stage;

Constraints: mass flux $\dot{m} \geq \dot{m}$ (baseline), total pressure ratio $\pi^* \geq \pi^*$ (baseline);

Design Variables: 20 variables on 5 spanwise sections, each section has 3 curvature control point values and 1 position value for one of the control points;

Genetic Algorithm (GA) parameters: the maximum iteration is 100, and the population size is 12.

In view of the error of inlet angles, as an empirical parameter, which is inherent and inevitable in 3D blade design, the optimization of the leading edge blade angles is essential in order to ameliorate the capacity of the fan stage in organizing viscous fluid. Similarly, the following are these optimization constraint conditions:

Maximize: adiabatic efficiency η^* on the highest efficiency point for fan stage;

Constraints: mass flux $\dot{m} \geq \dot{m}$(baseline), total pressure ratio $\pi^* \geq \pi^*$(baseline);

Design Variables: 5 variables defining the added metal angle $\Delta\beta$ at blade leading edge;

Genetic Algorithm (GA) parameters: the maximum iteration is 100, and the population size is 12;

Constants: all other parameters from the former optimization step.

A comparison of the aerodynamic performance achieved by different optimization strategies is shown in Table 3. The fan's aerodynamic performance is greatly enhanced by the two optimization steps. The adiabatic efficiency and the total pressure ratio of the fan stage are improved by 3.87% and 2.38% in the first step of optimization by Cam-ber_Opt respectively. Additionally, the mass flow rate is increased by 4.14%, which shows that the fan passage's capacity for organizing viscous fluid is significantly improved and the shear/expansion flow is diminished in the boundary layer. Based on Camber_Opt, the Angle_Opt is adopted to ameliorate the fan stage's aerodynamic performance. According to Table 3, the stage pressure ratio of the final design reaches 2.15, while the mass flow rate and the adiabatic efficiency are 9.45 kg/s and 0.891, respectively. With these results, it is safe to conclude that a more rational structure of the flow is realized by the optimizations of the camber line and the inlet angle, thereby realizing better organization of the viscous fluid while enhancing the overall performance of the whole stage.

Table 3. Aerodynamic performance for different design cases.

	Mass flux $\dot{m}$ (kg/s)		**Pressure Ratio π^* (−)**		**Efficiency η^* (−)**	
	Value	**(%)**	**Value**	**(%)**	**Value**	**(%)**
Baseline	8.94	0	2.10	0	0.853	0
Camber_Opt	9.31	+4.14	2.15	+2.38	0.886	+3.87
Angle_Opt	9.45	+5.70	2.15	+2.38	0.891	+4.45

Figure 3 displays the spanwise distributions of several aerodynamic characteristics at the rotor blade outlet. Discussion about these parameters could help determine the specific contribution rotor optimization has made. Figure 3a shows how to improve the camber line to significantly increase the adiabatic efficiency of the rotor blade, particularly in regions where $h/H > 60\%$. The efficiency can also be increased even further by matching the leading

edge angles, but the improvement is still marginal. These results suggest that the camber line optimization could reduce the shear flow downstream while weakening the shock wave intensity in the rotor channel, lowering the loss caused by the shock wave and the following boundary layer separation.

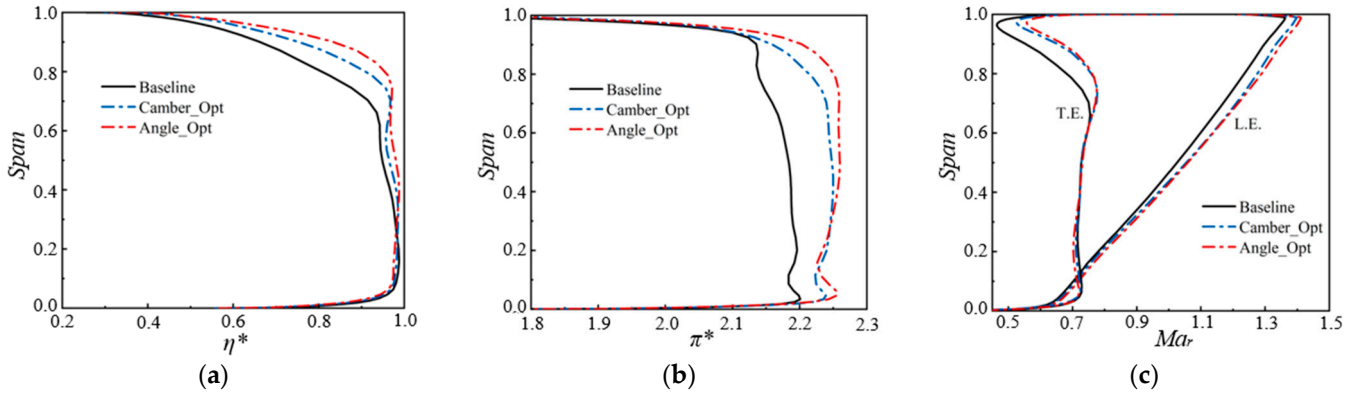


Figure 3. Comparisons of aerodynamic parameters for the rotor blade: (**a**) Adiabatic efficiency; (**b**) Total pressure ratio; (**c**) Relative Mach number.

The total pressure ratio of the rotor blade is evidently improved in the regions be-tween 20%*H*/*h* and 90%*H*/*h* following the camber line adjustment, according to the total pressure ratio described in Figure 3b compared to the baseline case. Moreover, Angle_Opt could further increase the pressure rise capability of the rotor blade on the basis of Camber_Opt. It can be concluded from these results that aerodynamic optimization design method in this paper is a highly recommendable one through which higher aerodynamic loading level could be obtained while maintaining the high efficiency.

As shown in Figure 3c, the increased axial flow velocity in the top half of the rotor blade is primarily responsible for the improved through-flow capacity of the fan stage. On the one hand, the increment of M_{ar} keeps rising along the blade's leading edge from hub to shroud. On the other hand, M_{ar}'s apparent improvement is only seen from 60% *H*/*h* to the blade's trailing edge. Abovementioned phenomena indicate that rotor optimization mainly works on the transonic region at the upper half of the blade, i.e., the positions where the shock wave occupy. All these results have proved the optimization of the rotor blade to be an effective method to improve the aerodynamic performance of the fan stage.

As we know, the transonic fan stage's aerodynamic performance is primarily influenced by the intensity and structure of the shock wave. The comparison of the on-wall isentropic Mach number for different cases is shown in Figure 4 in light of the fact that the shock wave's characteristics would be well mirrored by the isentropic Mach number. Results reveal that the position for the peak of M_{is} gets closer to the downstream after Camber_Opt, indicating that the shock wave on the blade suction surface is delayed. Moreover, the delay of the shock wave in the rotor blade passage could expand the throttling range of the transonic fan, which highlights the advantage of the design technique. After camber line optimization, the maximum value of M_{is} is also reduced, indicating that the shock wave's intensity has also been weakened. One of the other notable defections in the baseline configuration is the deviation of incidence angle which presented as the crossing of the M_{is} line at the blade leading edge. This problem is solved completely by Angle_Opt. In fact, although the position of the shock wave in Angle_Opt is moved slightly upstream compared with Camber_Opt, the location of the shock wave is still in the downstream in comparison with the baseline case, and the flow characteristics at the blade leading edge are improved greatly. In fact, near the rear region of the shock wave, the isentropic Mach number is decreased by Angle_Opt, which indicates that the rotor would have a better pressure rise capability.

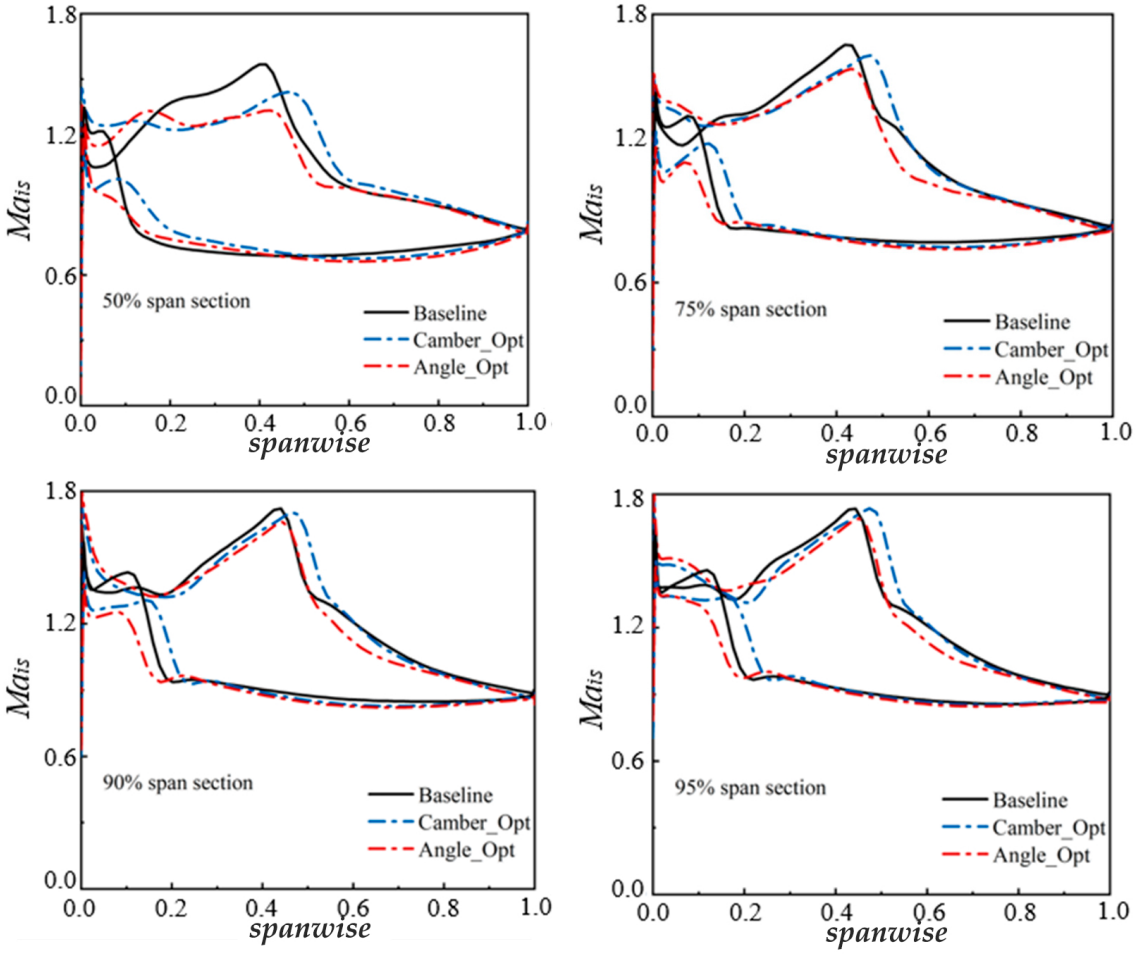


Figure 4. Isentropic Mach number on the surface of rotor blade.

Furthermore, the enhancement of pressure rise also comes from the changes in blade geometry. The comparison of rotor blade profiles at several spanwise sections is given in Figure 5. It can be seen that the optimized case's blade camber angle is less than that of the baseline case in areas above 40%H, particularly in the tip regions. The curvature at the blade's leading edge is decreased as well, which helps to reduce the camber angle and make contributions to shock wave control. The maximum deflection of the camber line is after 50%C_m, which is in line with the design concept of the high-load transonic fan.

Last but not least, the performance map of the fan stage is shown in Figure 6, along with the numerical and experimental results of a fan stage with the same flow path as the present fan [40]. Optimization of the rotor blade not only improves the performance of the fan stage at the design point, but also significantly improves the performance in off-design conditions. A notable increase in the chock mass flux is achieved by the optimization, which could greatly extend the stall margin of the fan stage. Moreover, based on the identical changing trend of both numerical and experimental results, the simulation results are within the margin of error, and hence it can be concluded that the numerical method adopted in the present study is reliable and has good accuracy.

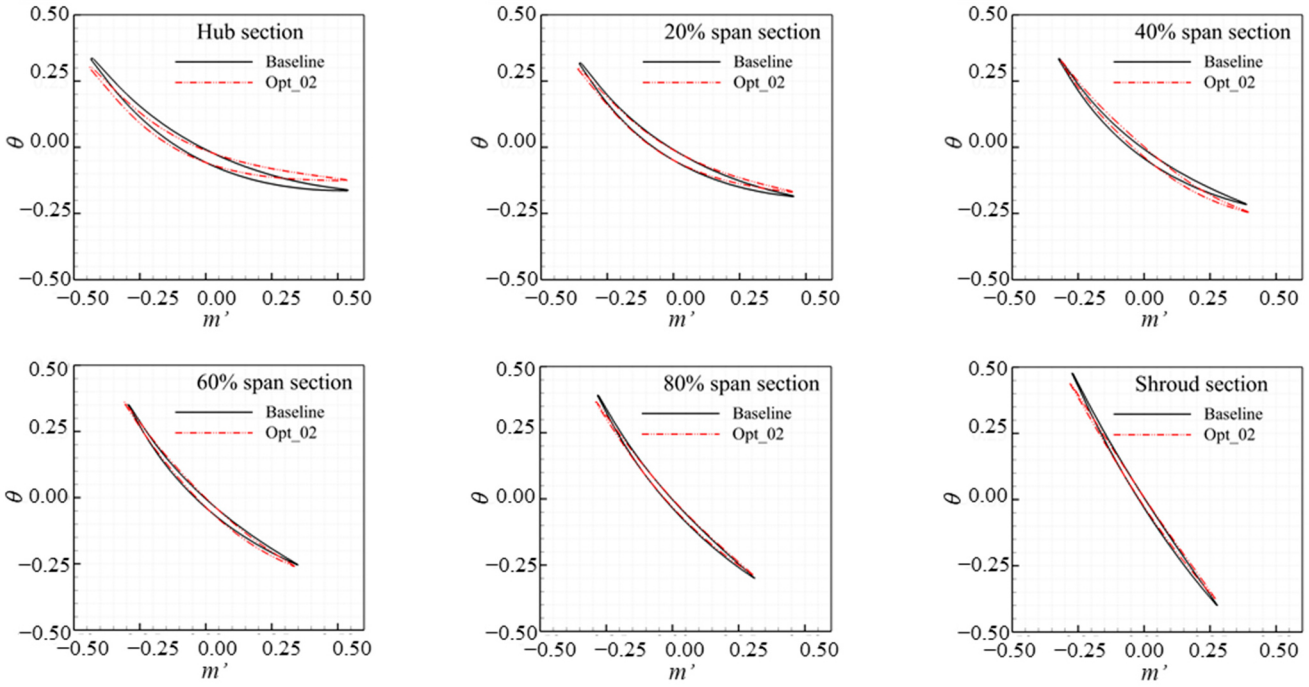


Figure 5. Blade profiles for the baseline and optimized rotor.

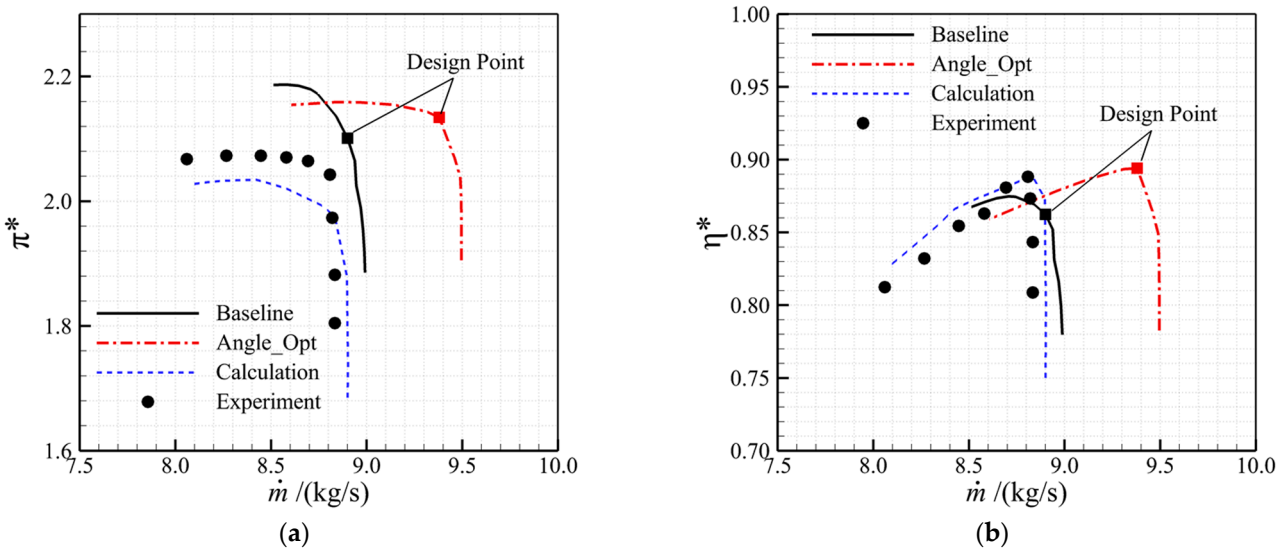


Figure 6. Performance map for the fan stage: (**a**) The total pressure ratio vs. mass flow rate; (**b**) The adiabatic efficiency vs. mass flow rate.

4. Vorticity Dynamics Diagnosis

This section examines the physical processes controlling boundary layer separation and shock waves from the perspective of vorticity dynamics. As an important ramification in fluid dynamics, vorticity dynamics mainly focuses on the derivative/gradient of flow parameters and could be used to examine major flow information while detecting the dynamic processes. Here, the physical cause of the curvature control-induced performance increase for the fan stage will be thoroughly studied, and the mechanism of the vorticity dynamics diagnosis method will be clearly understood.

4.1. Mathematical Explicit Relation between Vorticity Dynamics Parameters vs. Performance Parameters

To begin with, the relationship between the vorticity dynamics parameters and the throughflow capability of axial fan/compressor is investigated. All the discussion in this section is under the cylindrical coordinates system with the z-axis being the rotation axis, as shown in Figure 7.

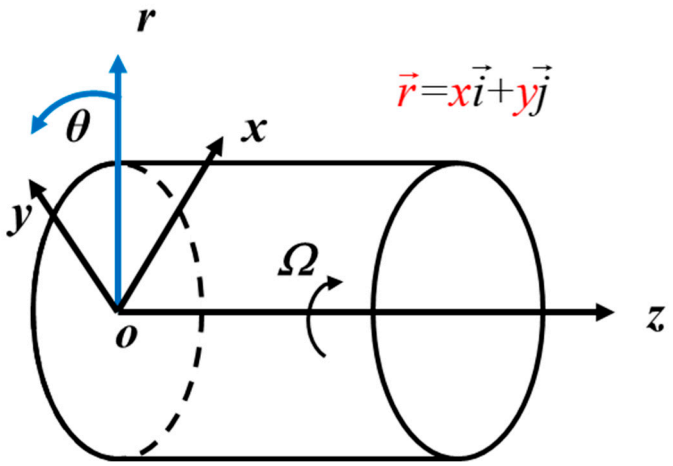


Figure 7. Cylindrical coordinates system.

As we know, the mass flux of an axial fan/compressor in the cylindrical coordinates can be read as follows:

$$\begin{aligned}\int_s \rho u_z dS &= \int_s \rho u_z r dr d\theta = \frac{1}{2}\left[\int_0^{2\pi} \rho u_z r^2 \Big|_{r_1}^{r_2} d\theta - \int_s r\frac{\partial \rho u_z}{\partial r} dS\right] = -\frac{1}{2}\int_s r\frac{\partial \rho u_z}{\partial r} dS \\ &= -\frac{1}{2}\int_s r\left(u_z\frac{\partial \rho}{\partial r} + \rho\frac{\partial u_z}{\partial r}\right)dS = -\frac{1}{2}\int_s r\left[u_z\frac{\partial \rho}{\partial r} + \rho\left(\frac{\partial u_r}{\partial z} - \omega_\theta\right)\right]dS\end{aligned} \tag{1}$$

Here, ω_θ denotes the azimuthal vorticity and is defined as:

$$\omega_\theta = \frac{\partial u_r}{\partial z} - \frac{\partial u_z}{\partial r} \tag{2}$$

Based on the fact that the $\partial\rho/\partial r$ and $\partial u_r/\partial z$ are ignorable at the inlet or outlet plane of fan/compressor, the Equation (1) could be simplified as:

$$\int_s \rho u_z dS \approx \frac{1}{2}\int_s r\rho\omega_\theta dS \tag{3}$$

Equation (3) indicates that the mass flux of the fan/compressor depends directly on the azimuthal vorticity ω_θ. Moreover, according to Equation (2), in the core flow region of the blade passage, $\partial u_r/\partial z \approx \partial u_z/\partial r \approx 0$, so $\omega_\theta \approx 0$. In the hub region where $\partial u_r/\partial z << \partial uz/\partial r$ and $\partial u_z/\partial r > 0$, $\omega_\theta \approx -\partial u_z/\partial r < 0$. In the casing region where $\partial u_r/\partial z << \partial u_z/\partial r$ and $\partial u_z/\partial r < 0$, $\omega_\theta \approx -\partial u_z/\partial r > 0$. Consequently, in order to improve the throughflow capability of the compressor, the reduction of area for the vortex regions near the hub and the casing is required. In other words, the increase of the mass flow rate calls for the decrease of the boundary layer thickness, which is in consistence with the general principle of fluid dynamics.

Using similar numerical methods, we can get the relation between other performance parameters and the vorticity parameters, as listed below:

(a) The relation between total pressure ratio and the azimuthal vorticity:

$$\begin{aligned}\pi_{tt} &= \frac{p_2^*}{p_1^*} = \frac{\frac{\int_{S_2}\rho u_z p^* dS}{\int_{S_2}\rho u_z dS}}{\frac{\int_{S_1}\rho u_z p^* dS}{\int_{S_1}\rho u_z dS}} = \frac{\frac{\int_{S_2}\rho u_z p^* dS}{\dot{m}_2}}{\frac{\int_{S_1}\rho u_z p^* dS}{\dot{m}_1}} = \frac{\int_{S_2}\rho u_z p^* dS}{\int_{S_1}\rho u_z p^* dS} = \frac{\int_{S_2}\rho u_z p^* dS}{C_1} \\ &= \frac{-\int_{S_2} r\rho p^* \frac{\partial u_z}{\partial r} dS}{2C_1} \approx \frac{\int_{S_2} r\rho p^* \omega_\theta dS}{C_2}\end{aligned} \tag{4}$$

$$\begin{aligned}C_2 &= 2C_1 = \int_{S_1}\rho u_z p^* dS \approx -0.5\int_{S_1} r\rho p^* \frac{\partial u_z}{\partial r} dS \\ &= -\pi\int_{r_1}^{r_2} r^2 \rho p^* \frac{\partial u_z}{\partial r} dr \approx \pi\int_{r_1}^{r_2} r^2 \rho p^* \omega_\theta dr\end{aligned} \tag{5}$$

(b) The relation between total temperature ratio and the azimuthal vorticity:

$$\begin{aligned}\tau_{tt} &= \frac{T_2^*}{T_1^*} = \frac{\frac{\int_{S_2}\rho u_z T^* dS}{\int_{S_2}\rho u_z dS}}{\frac{\int_{S_1}\rho u_z T^* dS}{\int_{S_1}\rho u_z dS}} = \frac{\frac{\int_{S_2}\rho u_z T^* dS}{\dot{m}_2}}{\frac{\int_{S_1}\rho u_z T^* dS}{\dot{m}_1}} = \frac{\int_{S_2}\rho u_z T^* dS}{\int_{S_1}\rho u_z T^* dS} = \frac{\int_{S_2}\rho u_z T^* dS}{C_3} \\ &= \frac{-\int_{S_2} r\rho T^* \frac{\partial u_z}{\partial r} dS}{2C_3} = \frac{\int_{S_2} r\rho T^* \omega_\theta dS}{C_4}\end{aligned} \tag{6}$$

$$\begin{aligned}C_4 &= 2C_3 = \int_{S_1}\rho u_z T^* dS \approx -0.5\int_{S_1} r\rho T^* \frac{\partial u_z}{\partial r} dS \\ &= -\pi\int_{r_1}^{r_2} r^2 \rho T^* \frac{\partial u_z}{\partial r} dr \approx \pi\int_{r_1}^{r_2} r^2 \rho T^* \omega_\theta dr\end{aligned} \tag{7}$$

(c) The relation between adiabatic efficiency and the azimuthal vorticity:

$$\eta_{tt} = \frac{\left(\frac{p_2^*}{p_1^*}\right)^{\frac{\gamma-1}{\gamma}} - 1}{\frac{T_2^*}{T_1^*} - 1} = \frac{\pi_{tt}^{\frac{\gamma-1}{\gamma}} - 1}{\tau_{tt} - 1} \approx \frac{\left(\frac{\int_{S_2} r\rho p^* \omega_\theta dS}{C_2}\right)^{\frac{\gamma-1}{\gamma}} - 1}{\frac{\int_{S_2} r\rho T^* \omega_\theta dS}{C_4} - 1} \tag{8}$$

(d) The relation between stall margin and the azimuthal vorticity:

$$SM = \frac{\frac{(\pi_{tt})_s}{(\pi_{tt})_d}}{\frac{(\dot{m})_s}{(\dot{m})_d}} - 1 \approx \frac{\left(\frac{\int_{S_2} r\rho p^* \omega_\theta dS}{C_2}\right)_s}{\left(\frac{\int_{S_2} r\rho p^* \omega_\theta dS}{C_2}\right)_d} - 1 = \frac{\left(\frac{\int_{S_2} r\rho p^* \omega_\theta dS}{C_2}\right)_s}{\left(\frac{\int_{S_2} r\rho p^* \omega_\theta dS}{C_2}\right)_d} \frac{\left(\int_S r\rho\omega_\theta dS\right)_d}{\left(\int_S r\rho\omega_\theta dS\right)_s} - 1 \tag{9}$$

Here, superscript * denotes the total condition, subscript *tt* denotes the total to total condition, while subscripts *s* and *d* represent the stall point and the design point, respectively.

To further reveal the mechanism of flow loss generation and find out the internal correlation between the vorticity and the compressor performance, the Boundary Vorticity Flux (BVF) is investigated in the present study. The concept of BVF was first put forward

by Lighthill [41] in 1963 as a measurement for the physical generation of vorticity in the on-wall area. Following is its definition:

$$\sigma = \frac{\mu}{\rho} n \cdot \nabla \omega = \nu \frac{\partial \omega}{\partial n} \tag{10}$$

The axial moment exerted on the gas by the rotor blades of an axial fan/compressor can be represented as follows:

$$M_z = -\int_S (r \times np)_z dS \tag{11}$$

Considering a sequence of mathematical transformation relations, Equation (11) could be transformed into the following form:

$$M_z = -\int_S (r \times np)_z dS = -\frac{1}{2}\int_{S_b} \rho r^2 \sigma_{pz} dS + \frac{1}{2}\oint_{\partial S_b} pr^2 dz \tag{12}$$

Here, M stands for total moment vector of acting onto the fluid by fan/compressor rotor blades, and M_z is its axial-component. σ_{pz} is axial-component of BVFσ_p, S_b denotes rotor blade surface and ∂S_b is the boundary of S_b. According to Equation (12), the M_z consists of two parts: the surface integration of the second-moment of σ_{pz} is the first part, and the curve integration of the second-moment of static pressure p is the second. Hence, we can see that the lower σ_{pz} is, the higher M_z will be, which would have more beneficial effects on the total pressure ratio for the fan/compressor rotor blade passage. Therefore, the axial component of the BVF σ_{pz} is an important parameter that reflects the aerodynamic performance of the fan/compressor.

4.2. Flow Diagnosis Based on Vorticity Dynamics

The distribution of azimuthal vorticity between the baseline and the optimized case is presented in Figure 8. Four sections are displayed, as shown in Figure 9, the chord-wise locations are c/C_m = 14%, c/C_m = 42%, c/C_m = 70% and c/C_m = 90%, respectively. Compared with the baseline case, significant reduction of the vortex intensity is achieved by the optimization, which is particularly obvious in the tip region of the rotor blade. This phenomenon further demonstrates that the rotor optimization could obtain a more reasonable configuration of the shock wave in the transonic fan, which would therefore enhance the through flow capability according to Equation (3).

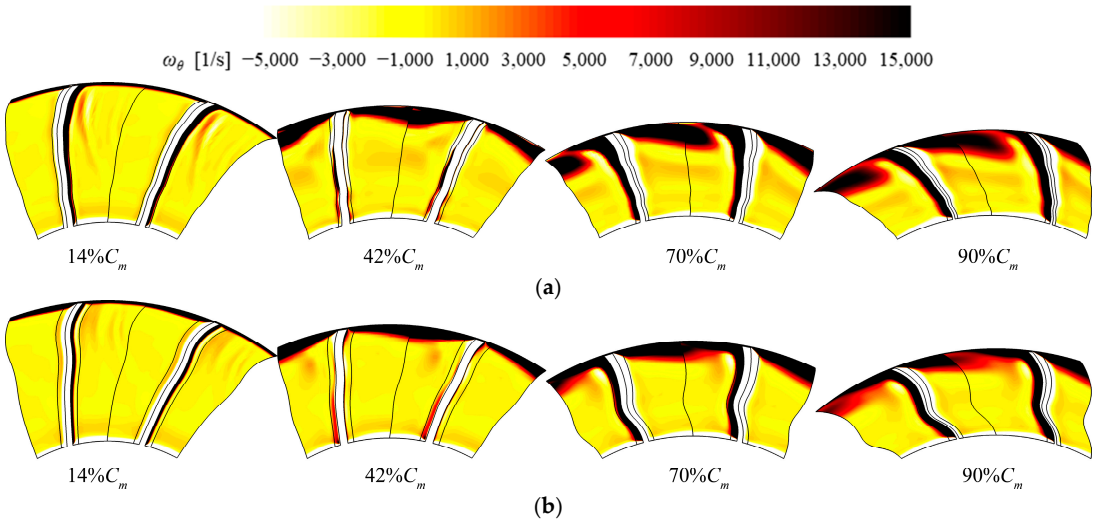


Figure 8. Azimuthal vorticity in cross section in the rotor passage: (**a**) Baseline; (**b**) Optimized.

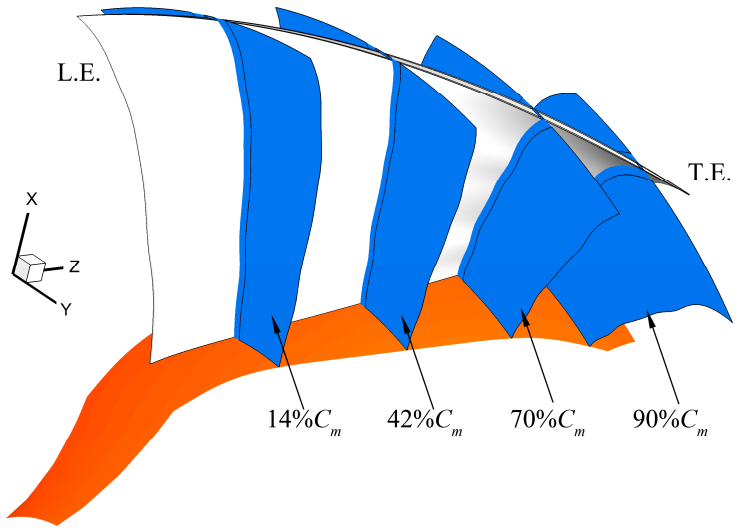


Figure 9. Chordwise location for cross sections in the rotor.

Presented in Figure 10, the radial vorticity and the skin-friction lines on the rotor blade suction surface demonstrate that boundary-layer separation caused by shock wave features as a sharp decrease in the radial vorticity, and since the optimized rotor has a smaller separation region, it has a weaker radial vorticity gradient. The weakened separation flow indicates that the optimized rotor blade in this study could achieve a favorable control effect on the shock wave in the upper half of the blade, whereby improving the aerodynamic performance of the fan stage. However, the negative radial vorticity near the hub at the inlet of the optimized rotor blade indicates the lack of accuracy in leading edge metal angle at these areas, which needs to be further optimized in future studies.

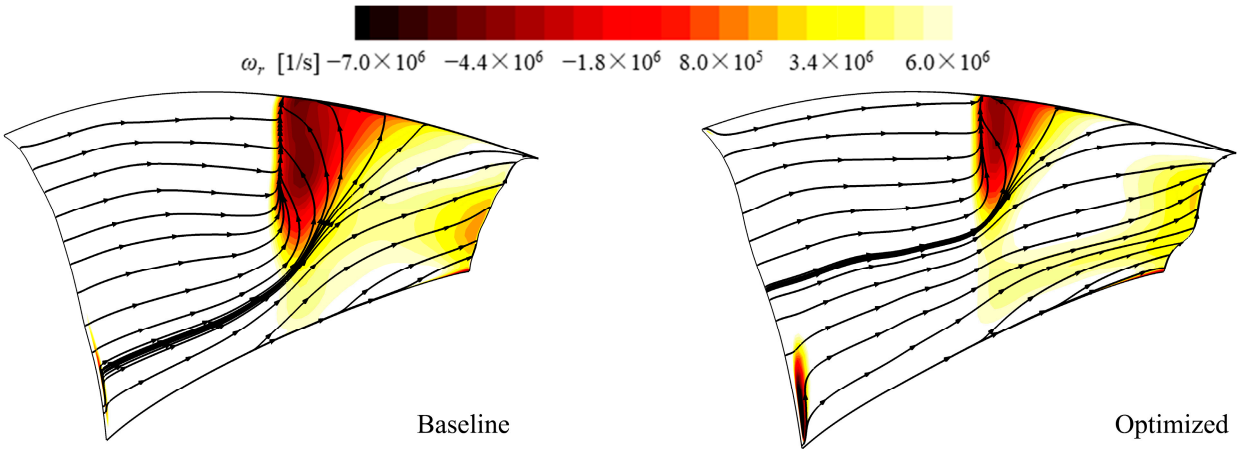


Figure 10. Radial vorticity and skin-friction lines on the blade suction surface.

The axial component of BVF (σ_{pz}) on the blade suction surface is shown in Figure 11. According to the demonstrations above, the increment of σ_{pz} in the boundary layer area is detrimental to the performance of the compressor due to the reduction in the total aerodynamic torque. As can be seen in Figure 11, the positive peak of σ_{pz} is weakened and shifted towards the upper part of the blade in the optimized case, which indicates that the flow loss caused by the shock wave is reduced significantly, and the fluid will be able to receive larger axial torque when it travels through the rotor blade passage.

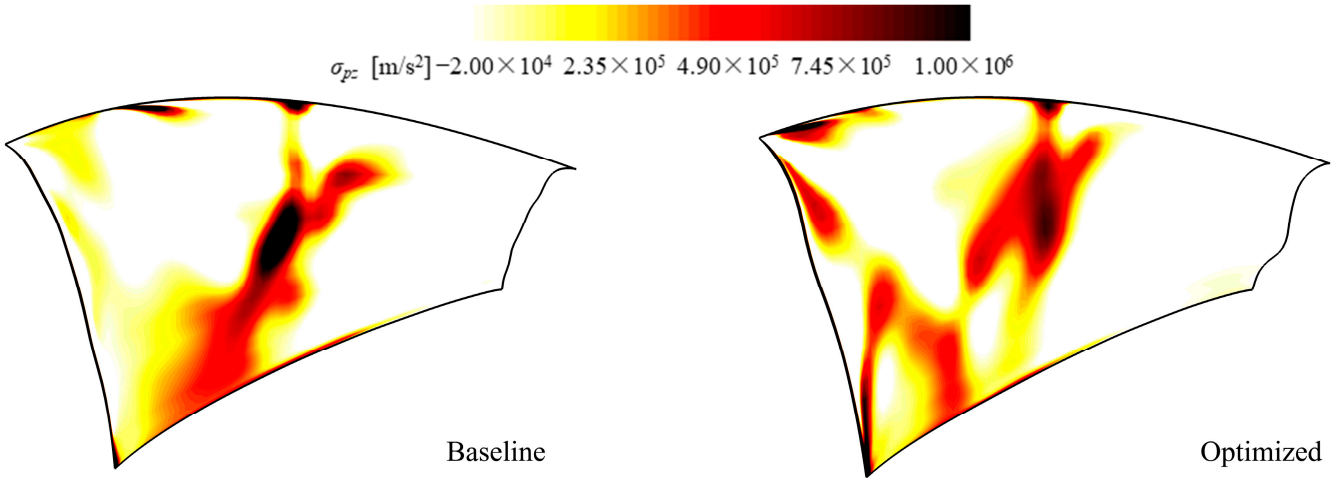


Figure 11. BVF-σ_{pz} on rotor suction surface.

According to the famous boundary layer separation criteria proposed by Wu [26] (although there have been some long-standing controversial issues), boundary layer separation is characterized by the following three features:

Separation zone warning: The distinctive vorticity vector lines on the wall have a significant positive curvature in addition to converging skin-friction lines.

Separation line criteria: The curvature of vorticity lines reach a maximum.

Separation watch: Tangent BVF lines turn to the direction of skin-friction lines on wall, or the tangent pressure gradient vector lines are basically perpendicular to the separation line.

Above criteria are employed to investigate the flow in the present rotor blade passage. The skin-friction lines and the BVF lines are presented in Figure 12. The range of the shock-wave-induced separation bubble which is sketched clearly by the skin-friction lines is reduced significantly in the optimized case, and the direction of the BVF lines is just in parallel with the separation line, which is in good agreement with the above-mentioned criteria.

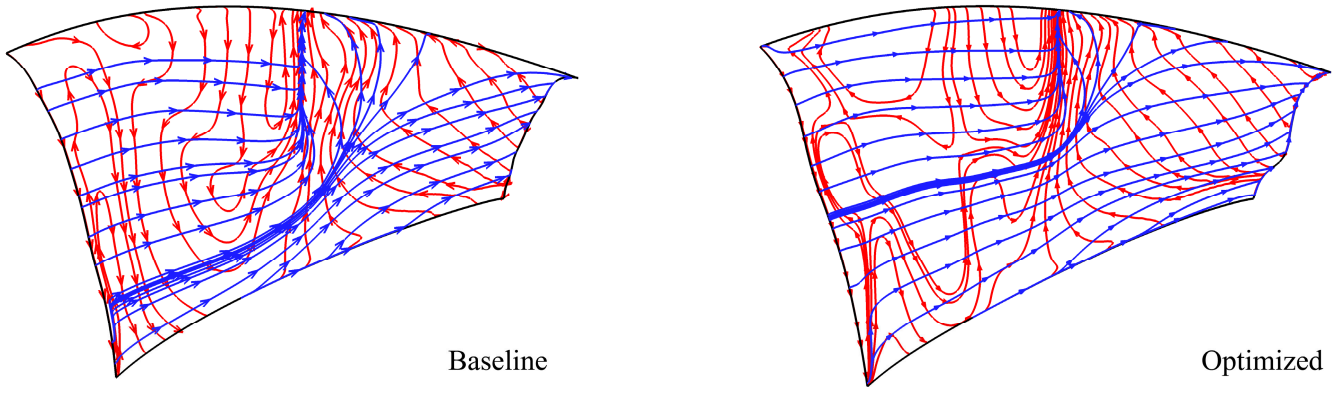


Figure 12. BVF lines (in red) on and skin-friction lines (in blue) on rotor blade suction side.

The specific entropy and its gradient on the rotor blade suction surface are presented in Figure 13, the vector lines (τ, ω) are depicted as well. For the optimized case, entropy production caused by the shock wave in the tip region of the rotor blade is reduced remarkably, and the flow separation is suppressed effectively. In fact, the fundamental principle of transonic fan optimization design is the control and utilization of the shock wave. According to Figure 13b, the spike of entropy gradient coincides well with the separation line, which is more helpful to examine boundary-layer separation. Also, the reduction of the entropy gradient in the vicinity of the separation line indicates that the

intensity of the shock wave is weakened effectively by the optimization of the curvature. Moreover, it can be seen that on both sides of separation line where the skin-friction lines converge, the curvature of the vorticity lines reaches its peak, which proves to be a valid method to identify boundary-layer separation flow.

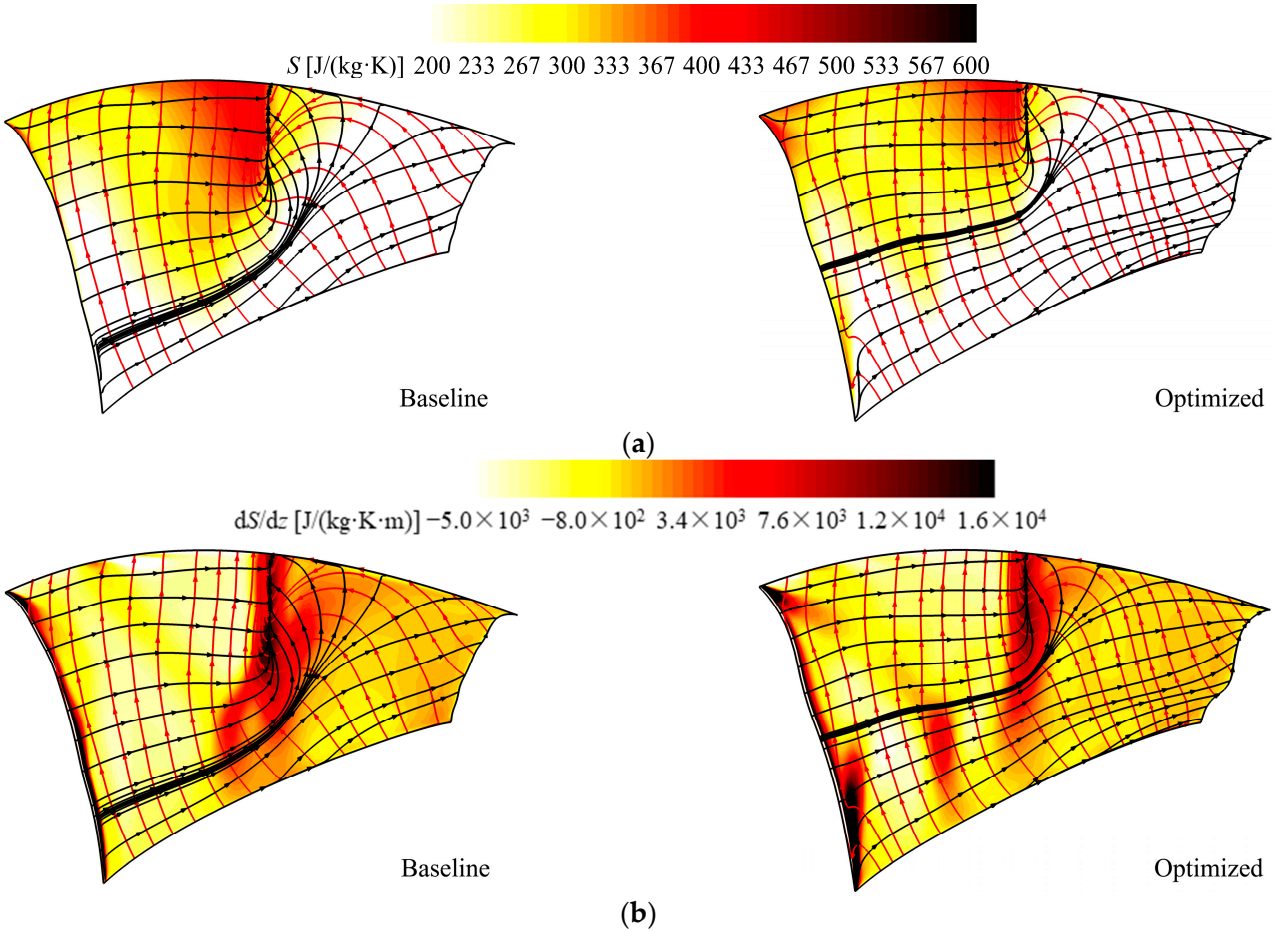


Figure 13. Vector lines (τ, ω) and entropy on the rotor blade suction side: (**a**) Vector lines (τ, ω) and specific entropy; (**b**) Vector lines (τ, ω) and axial gradient of entropy.

Designed to compress fluid, the main goal of a fan stage is to increase the static pressure of the fluid that flows through its blade passages. The static pressure on the suction surface of the rotor blade is presented in Figure 14a, and the gradient of the static pressure is shown in Figure 14b. As shown in Figure 14a, the static pressure in the upstream of the separation region is higher in the optimized case than that in the baseline case, which indicates that the Mach number in front of the shock wave is lowered by the optimization. As a result, the intensity of the shock wave will be weakened and the consequent shock loss will be reduced. The gradient of the static pressure in Figure 14b has also demonstrated that gradient of the static pressure is more beneficial to check shock wave and boundary-layer separation. Moreover, the shock wave is weakened remarkably for the optimized case, which provides a more reasonable flow configuration in the rotor blade passage.

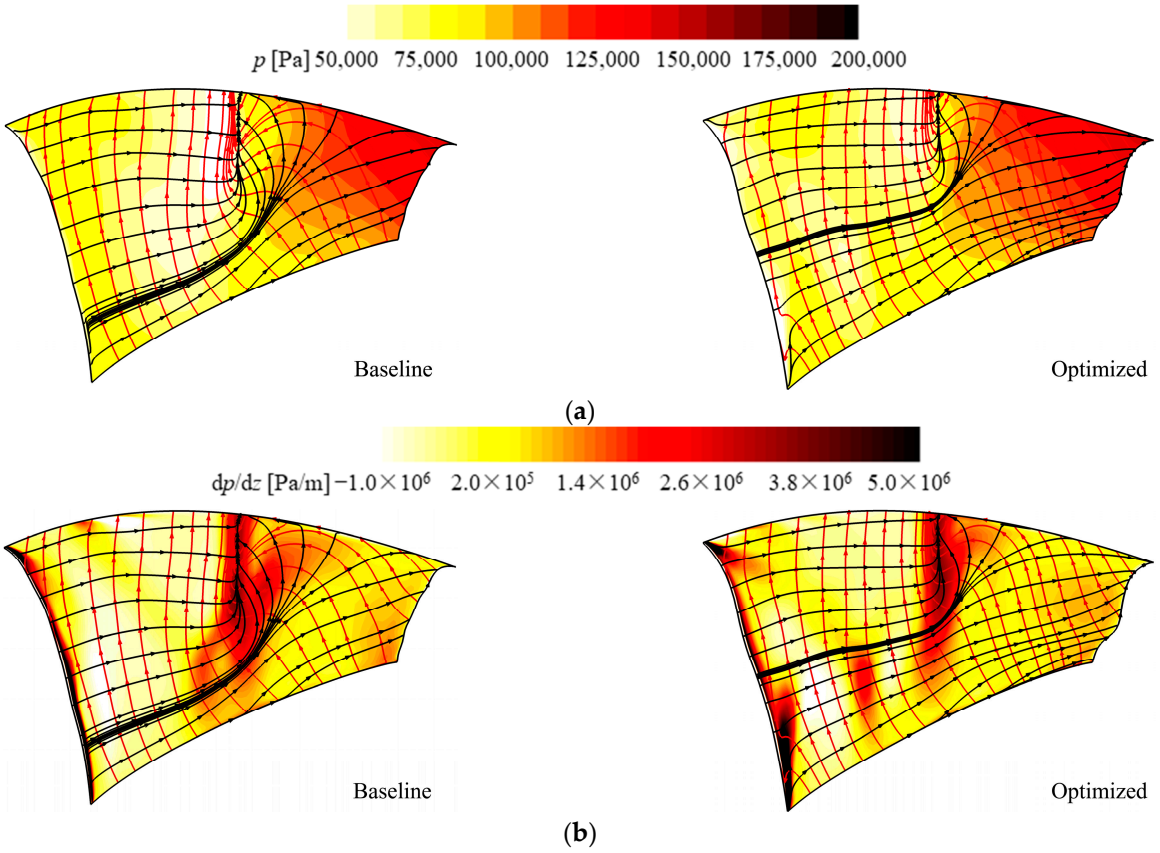


Figure 14. Vector lines (τ, ω) and static pressure on the rotor blade suction side: (**a**) Vector lines (τ, ω) and specific static pressure; (**b**) Vector lines (τ, ω) and axial gradient of static pressure.

5. Conclusions

The aerodynamic optimization of the rotor blade in a low-bypass transonic fan stage is implemented, and a flow diagnostic method based on vorticity dynamics is employed in order to discuss the flow and reveal the mechanism of three-dimensional transonic flow both in the baseline and optimized fan blade passage.

By optimizing the curvature of the camber line and matching the inlet flow angle, a novel rotor blade geometry with continuous curvature is acquired. As a result, the intensity and scale of the shock wave are reduced and the subsequent boundary layer flow separation is delayed, increasing the through-flow effect and pressure rise effect while reducing flow loss level in the optimized transonic fan stage passage. After the optimization, the total pressure ratio of the fan stage is increased by 1.90%, while the adiabatic efficiency and mass flow rate are increased by 4.45% and 5.82%, respectively.

The aerodynamic performance of axial flow fan/compressor depend strongly on the vorticity dynamic parameters revealed from vorticity dynamic theory formulas in this research. The azimuthal vorticity and the boundary vorticity flux have significant influences on the through-flow effect and other aerodynamic performance parameters of the fan/compressor passage. The triggering of boundary layer flow separation in a transonic fan passage is accompanied by the spike of entropy and static pressure, and their derivative/gradient values will also be changed drastically. Other than flow parameters themselves, the derivative/gradient of flow parameters can reveal more underlying and higher accuracy information to researchers. Thus, the utilization of flow diagnostic method based on vorticity dynamics can provide the researchers with a novel method for turbomachinery aerodynamic analysis and design in the aero-engine engineering development field.

Author Contributions: Conceptualization, M.L.; Methodology, Z.Z. and H.X.; Validation, Z.L. and X.Y.; Resources, H.C.; Writing—original draft, M.L. and Z.Z.; Writing—review & editing, H.C.; Visualization, C.S. All authors have read and agreed to the published version of the manuscript.

Funding: This work was supported by the grant from the Scientific research platform and projects of colleges and universities of Guangdong Province Department of Education (Grant No. KJ2022C010), the Guangdong Provincial Science and Technology Plan Project (Grant No. 2021A0505030013, No. 2023ZDZX3082) and National Science and Technology Major Project (No. J2019-II-0016-0037).

Data Availability Statement: Not applicable.

Conflicts of Interest: The authors declare no conflict of interest.

Nomenclature

c	Local meridian curve distance
C_m	Total meridian curve distance
h	Local span distance
H	Blade height
m'	Normal coordinate for the streamline
$\dot{m}$	Mass flow rate
Ma	Mach number
M	Moment vector, Mach number
$\overline{n}$	Corrected Rotating speed
p	Pressure
r	Radial coordinates
S	Entropy
T	Temperature
u	Non-dimensional coordinate in basic airfoil plane, absolute velocity
z	Axial coordinates
α	Out flow angle
$\Delta\beta$	viation on metal angle
δ	Deviation angle
η	Efficiency
θ	Circumferential coordinates
$\Delta\theta$	Deviation on tangential lean angle
μ	Dynamic viscosity
ν	Kinematic viscosity
π	Pressure ratio
ρ	Density
σ_p	Boundary vorticity flux
τ	Shear stress
ω	Vorticity
Subscripts/Superscripts	
1	Inlet conditions
2	Outlet conditions
r	Relative conditions
r, θ, z	Radial, circumferential, axial components
is	Isentropic
*	Total condition

References

1. Wu, C.H. *A General Theory of Three-Dimensional Flow in Subsonic and Supersonic Turbomachines of Axial-, Radial, and Mixed-Flow Types*; Rept. NACA-TN-2604; National Aeronautics and Space Administration: Cleveland, OH, USA, 1952.
2. Novak, R.A. Streamline Curvature Computing Procedures for Fluid-Flow Problems. *J. Eng. Power* **1967**, *89*, 478–490. [CrossRef]
3. Marsh, H.A. *Digital Computer Program for the Through-Flow Fluid Mechanics in an Arbitrary Turbomachine Using a Matrix Method*; Her Majesty's Stationery Office: London, UK, 1966.
4. Bliss, D.; Hayden, R.; Murray, B.; Schwaar, P. Design Considerations for a Novel Low Source Noise Transonic Fan Stage. In Proceedings of the 3rd Aeroacoustics Conference, Aeroacoustics Conferences, Palo Alto, CA, USA, 20–23 July 1976, AIAA Paper No. 76-577. [CrossRef]

5. Lucas, J.; Woodward, R.; Mackinnon, M. Acoustic Evaluation of a Novel Swept Rotor Fan. In Proceedings of the 11th Fluid and Plasma Dynamics Conference, Fluid Dynamics and Co-located Conferences, Seattle, WA, USA, 10–12 July 1978, AIAA Paper No. 78-1121. [CrossRef]
6. Wennerstrom, A.J.; Frost, G.R. Design of a 1500ft/sec, Transonic, High-Through-Flow, Single-Stage Axial-Flow Compressor with Low Hub/Tip Ratio; Air Force Aero Propulsion Lab, Wright-Patterson AFB: Dayton, OH, USA, 1976; No. AFARL-TR-76-59. Available online: https://apps.dtic.mil/sti/citations/ADB016386 (accessed on 17 February 2023).
7. Wennerstrom, A.J.; Derose, R.D.; Law, C.H.; Buzzell, W.A. Investigation of a 1500ft/sec, Transonic, High-Through-Flow, Single-Stage Axial-Flow Compressor with Low Hub/Tip Ratio; Air Force Aero Propulsion Lab, Wright-Patterson AFB: Dayton, OH, USA, 1976; No. AFARL-TR-76-92. Available online: https://apps.dtic.mil/sti/citations/ADB016506 (accessed on 17 February 2023).
8. Frank, B.; King, P.; Copenhaver, W. Effects of Leading Edge Sweep on Stall Inception in a High-Speed Single-Stage Compressor. In Proceedings of the 30th Joint Propulsion Conference and Exhibit, Indianapolis, IN, USA, 27–29 June 1994, AIAA Paper No. 94-2696. [CrossRef]
9. Boyer, K.; King, P.; Copenhaver, W. Stall Inception in Single Stage, High-Speed Compressors with Straight and Swept Leading Edges. In Proceedings of the AIAA, SAE, ASME, and ASEE, 29th Joint Propulsion Conference and Exhibit, Monterey, CA, USA, 28–30 June 1993. [CrossRef]
10. Denton, J.D.; Xu, L. The Effects of Lean and Sweep on Transonic Fan Performance. In *ASME Turbo Expo 2002: Power for Land, Sea, and Air*; Paper GT 2002-30327; American Society of Mechanical Engineers: Amsterdam, The Netherlands, 2002; Volume 5, pp. 23–32. [CrossRef]
11. Shan, P.; Gui, X. *Final Report for the Design and Experiment Study of a High Loading Single-Stage Model Fan ATS-2 with a Backward Swept Rotor*; Rept. GF-A0041935; Beihang University: Beijing, China, 2000.
12. Hu, G.R.; Zhou, Y.F.; Chen, B.S.; Wei, Y.B. Design and Test for Single Stage Transonic Fan with High Speed, High Load. *J. Eng. Thermophys.* **2001**, *22*, 40–43.
13. Ceyrowsky, T.; Hildebrandt, A.; Schwarze, R. Numerical investigation of the circumferential pressure distortion induced by a centrifugal compressor's external volute. In Proceedings of the Turbo Expo 2018: Turbomachinery Technical Conference & Exposition, Oslo, Norway, 11–15 June 2018, ASME paper GT2018-75919.
14. Cravero, C.; Marsano, D.; Sishtla, V.; Halbe, C.; Cousins, W.T. Numerical Investigations of Near Surge Operating Conditions in a Two-Stage Radial Compressor with Refrigerant Gas. In Proceedings of the ASME Turbo Expo 2023: Turbomachinery Technical Conference and Exposition, Boston, MA, USA, 26–30 June 2023; Volume 87110, p. V13DT36A016.
15. Benini, E. Three-Dimensional Multi-Objective Design Optimization of a Transonic Compressor Rotor. *J. Propuls. Power* **2003**, *20*, 559–565. [CrossRef]
16. Jang, C.M.; Li, P.; Kim, K.Y. Optimization of Blade Sweep in a transonic Axial Compressor Rotor. *JSME Int. J. Ser. B* **2005**, *48*, 793–801. [CrossRef]
17. Lian, Y.; Liou, M.S. Multi-Objective Optimization of Transonic Compressor Blade Using Evolutionary Algorithm. *J. Propuls. Power* **2005**, *21*, 979–987. [CrossRef]
18. Ellbrant, L.; Eriksson, L.-E.; Martensson, H. Design of Compressor Blades considering Efficiency and Stability using CFD based Optimization. In *ASME Turbo Expo 2012: Turbine Technical Conference and Exposition*; Paper GT 2012-69272; American Society of Mechanical Engineers: Copenhagen, Denmark, 2012; Volume 8, pp. 371–382. [CrossRef]
19. Ellbrant, L.; Eriksson, L.E.; Martensson, H. Balancing Efficiency and Stability in the Design of Transonic Compressor Stages. In *ASME Turbo Expo 2013: Turbine Technical Conference and Exposition*; Paper GT 2013-94838; American Society of Mechanical Engineers: San Antonio, TX, USA, 2013; Volume 6B, p. V06BT37A017. [CrossRef]
20. Oyama, A.; Liou, M.S.; Obayashi, S. Transonic Axial Flow Blade Optimization Evolutionary Algorithms Three-Dimensional Navier-Stokes Solver. *J. Propuls. Power* **2004**, *20*, 612–619. [CrossRef]
21. Nemnem, A.F. A General Multidisciplinary Turbomachinery Design Optimization System Applied to a Transonic Fan. Ph.D. Theis, Department of Aerospace Engineering and Engineering Mechanics, University of Cincinnati, Cincinnati, OH, USA, 2014.
22. Siddappaji, K. Parametric 3D Blade Geometry Modeling Tool for Turbomachinery Systems. Master's Thesis, College of Engineering and Applied Science, University of Cincinnati, Cincinnati, OH, USA, 2012.
23. Nemnem, A.F.; Turner, M.G.; Siddappaji, K.; Galbraith, M. A Smooth Curvature-Defined Meanline Section Option for a General Turbomachinery Geometry Generator. In *ASME Turbo Expo 2014: Turbine Technical Conference and Exposition*; Paper GT 2014-26363; American Society of Mechanical Engineers: Düsseldorf, Germany, 2014; Volume 2B, p. V02BT39A026. [CrossRef]
24. Nemnem, A.F.; Turner, M.G.; Siddappaji, K.; Gannon, A.J. An Automated 3D Turbomachinery Design and Optimization System. *J. Multidiscip. Eng. Sci. Technol.* **2015**, *2*, 3345–3359.
25. Siddappaji, K.; Turner, M.G.; Dey, S.; Park, K.; Merchant, A. Optimization of a 3-Stage Booster: Part 2—The Parametric 3D Blade Geometry Modeling Tool. In *ASME Turbo Expo 2011: Turbine Technical Conference and Exposition*; Paper GT 2011-46664; American Society of Mechanical Engineers: Vancouver, BC, Canada, 2011; Volume 7, pp. 1431–1443. [CrossRef]
26. Siddappaji, K.; Turner, M.G.; Merchant, A. General Capability of Parametric 3D Blade Design Tool for Turbomachinery. In *ASME Turbo Expo 2012: Turbine Technical Conference and Exposition*; Paper GT 2012-69756; American Society of Mechanical Engineers: Copenhagen, Denmark, 2012; Volume 8, pp. 2331–2344. [CrossRef]
27. Turner, M.G.; Merchant, A.; Bruna, D. A Turbomachinery Design Tool for Teaching Design Concepts for Axial-Flow Fans, Compressors, and Turbines. *J. Turbomach.* **2011**, *133*, 937–952. [CrossRef]

28. Xia, L.; Zou, Z.J.; Wang, Z.H.; Zou, L.; Gao, H. Surrogate model based uncertainty quantification of CFD simulations of the viscous flow around a ship advancing in shallow water. *Ocean. Eng.* **2021**, *234*, 109206. [CrossRef]
29. Cravero, C.; De Domenico, D.; Marsano, D. Uncertainty Quantification Analysis of Exhaust Gas Plume in a Crosswind. *Energies* **2023**, *16*, 3549. [CrossRef]
30. Xiang, H.; Gao, J.; Hou, A.; Zhou, Y.; Yang, Y. Effect of atmospheric humidity on the aerodynamic performance of a transonic compressor cascade. *Gas Turbine Exp. Res.* **2020**, *33*, 1–7.
31. Zhang, G.; Yang, Y.; Chen, J.; Jin, Z.; Majkut, M.; Smołka, K.; Dykas, S. Effect of relative humidity on the nozzle performance in non-equilibrium condensing flows for improving the compressed air energy storage technology. *Energy* **2023**, *280*, 128240. [CrossRef]
32. Wiśniewski, P.; Majkut, M.; Dykas, S.; Smołka, K.; Zhang, G.; Pritz, B. Selection of a steam condensation model for atmospheric air transonic flow prediction. *Appl. Therm. Eng.* **2022**, *203*, 117922. [CrossRef]
33. Wiśniewski, P.; Zhang, G.; Dykas, S. Numerical investigation of the influence of air contaminants on the interfacial heat transfer in transonic flow in a compressor rotor. *Energies* **2022**, *15*, 4330. [CrossRef]
34. Bertoneri, M.; Duni, S.; Ransom, D.; Podestà, L.; Camatti, M.; Bigi, M.; Wilcox, M. Measured performance of two-stage centrifugal compressor under wet gas condition. In *Turbo Expo: Power for Land, Sea, and Air*; ASME GT2012-69819; American Society of Mechanical Engineers: New York, NY, USA, 2012.
35. Wu, J.Z.; Ma, H.Y.; Zhou, M.D. *Vorticity and Vortex Dynamics*; Springer: Berlin, Germany, 2006.
36. Wu, J.Z.; Tramel, R.W.; Zhu, F.L.; Yin, X. A vorticity dynamics theory of three-dimensional flow separation. *Phys. Fluids* **2000**, *12*, 1932–1954. [CrossRef]
37. Wu, J.Z.; Lu, X.Y.; Yang, Y.T.; Zhang, R.K. Vorticity dynamics in complex flow diagnosis and management. In Proceedings of the 13th Asian Congress Fluid Mechanics, Dhaka, Bangladesh, 17–21 December 2010; pp. 1–22.
38. Yang, Y.; Wu, H.; Li, Q.S.; Sheng, Z.; Wu, J.Z. Vorticity dynamics in axial compressor flow diagnosis and design. *J. Fluids Eng.* **2008**, *130*, 041102. [CrossRef]
39. Li, Q.S.; Wu, H.; Guo, M.; Wu, J.Z. Vorticity dynamics in axial compressor flow diagnosis and design—Part ii: Methodology and application of boundary vorticity flux. *J. Fluids Eng.* **2010**, *132*, 011102. [CrossRef]
40. Li, S. Design of Highly Loaded Dihedral Stator and Investigation on the Aerodynamic Stage Performance in an Axial Transonic Compressor. Ph.D. Thesis, Harbin Institute of Technology, Harbin, China, 2007.
41. Lighthill, M.J. *Laminar Boundary Layers*; Oxford University Press: Oxford, UK, 1963; pp. 46–113.

Disclaimer/Publisher's Note: The statements, opinions and data contained in all publications are solely those of the individual author(s) and contributor(s) and not of MDPI and/or the editor(s). MDPI and/or the editor(s) disclaim responsibility for any injury to people or property resulting from any ideas, methods, instructions or products referred to in the content.